Research Article | Vol. 27, No. 17 | 19 Aug 2019 | OPTICS EXPRESS 24455
Optics EXPRESS

Nonlocal collective ultrastrong interaction of plasmonic metamaterials and photons in a terahertz photonic crystal cavity

FANQI MENG,[1,2] MARK D. THOMSON,[1] BERNHARD KLUG,[1] DOVILĖ ČIBIRAITĖ,[1] QAMAR UL-ISLAM,[1] AND HARTMUT G. ROSKOS[1,3]

[1]*Physikalisches Institut, Johann Wolfgang Goethe-Universität, Max-von-Laue-Straße 1, D-60438 Frankfurt am Main, Germany*
[2]*fmeng@physik.uni-frankfurt.de*
[3]*roskos@physik.uni-frankfurt.de*

Abstract: Light-matter interaction in the strong coupling regime is of profound interest for fundamental quantum optics, information processing and the realization of ultrahigh-resolution sensors. Here, we report a new way to realize strong light-matter interaction, by coupling metamaterial plasmonic "quasi-particles" with photons in a photonic cavity, in the terahertz frequency range. The resultant cavity polaritons exhibit a splitting which can reach the ultra-strong coupling regime, even with the comparatively low density of quasi-particles, and inherit the high Q-factor of the cavity despite the relatively broad resonances of the Swiss-cross and split-ring-resonator metamaterials used. We also demonstrate nonlocal collective interaction of spatially separated metamaterial layers mediated by the cavity photons. By applying the quantum electrodynamic formalism to the density dependence of the polariton splitting, we can deduce the intrinsic transition dipole moment for single-quantum excitation of the metamaterial quasi-particles, which is orders of magnitude larger than those of natural atoms. These findings are of interest for the investigation of fundamental strong-coupling phenomena, but also for applications such as ultra-low-threshold terahertz polariton lasing, voltage-controlled modulators and frequency filters, and ultra-sensitive chemical and biological sensing.

1. Introduction

Strong light-matter interaction in a resonant cavity is at the core of quantum electrodynamics (cavity QED) research. It has been intensively studied for several decades, as it both reveals and exploits fascinating quantum-optical phenomena such as entanglement, and provides a promising approach to quantum computing and quantum information processing [1–5]. While the strong coupling regime of cavity QED was initially explored with atoms, it was later realized with a range of fermionic solid-state material systems, involving, for instance, interband (excitonic) or inter-subband transitions in quantum wells [6–8] and quantum dots [9,10]. It was also demonstrated with a bosonic superconducting two-level system coupled to a microwave superconducting transmission line resonator [11], and, most recently, with cyclotron transitions in 2D electron gases [12,13], spin resonances in magnetic materials [14–16] and molecular vibrational transitions in polymers [17,18]. Strong interaction between localized surface plasmons and photons in either waveguide or metallic cavity was also investigated in the visible/infrared spectral range [19–21]. However, the fundamental research and applications are limited in these experiments due to the nano-scale size of the required structures. In the terahertz frequency range, on the other hand, it is difficult to realize a cavity with simple metallic reflectors due to the strong Drude absorption of *free-carriers* in metal. Here, by employing a *dielectric* photonic crystal cavity [13], we realize the strong interaction between photons and plasmonic quasi-particles consisting of electromagnetic metamaterials

#368245 https://doi.org/10.1364/OE.27.024455
Journal © 2019 Received 24 May 2019; accepted 8 Jul 2019; published 13 Aug 2019

Optics EXPRESS

(MMs) in the terahertz frequency range, which opens new routes to take advantage of the rich functionalities of MMs and enables versatile applications in the terahertz frequency domain.

A MM is constructed by densely packing subwavelength-sized dielectric or metallic unit structures to manipulate the flow of electromagnetic waves with a high degree of precision [22]. By rational design of the subwavelength elements, a wide variety of optical functionalities can be achieved, such as chirality [23], negative refraction [24], total absorption [25,26] and cloaking [27,28]. In general, while the performances of MMs are demonstrated with classical light, there is also a growing interest in the investigation of the quantum properties of MMs [29–31]. Very recently, MMs were even employed to generate and manipulate entangled states of photons [32].

By placing planar plasmonic MMs in a one-dimensional (1D) terahertz photonic crystal (PC) cavity, we investigate strong coupling of these artificial atoms with the cavity photons. In the research field of cavity QED, one employs three key parameters to characterize the interaction of the cavity photons with the material: κ, γ, g, where κ and γ represent the population decay rates of the cavity photons and of the photo-excited state of the material, respectively, and g is the coupling strength where $2g$ represents the Rabi splitting. If $2g < (\gamma + \kappa)/2$, the interaction is in the weak-coupling regime, whereas for $2g > (\gamma + \kappa)/2$, one is within the limits of strong coupling. Furthermore, if the coupling strength reaches a sufficiently large fraction of the cavity mode's resonance frequency ω_c, such that the rotating-wave approximation of the theoretical treatment is no longer valid, one reaches the ultrastrong coupling regime (typically defined by $g/\omega_c > 0.1$). For even stronger coupling ($g/\omega_c \approx 1$) one speaks of the deep strong coupling regime [33,34]. A dimensionless parameter which describes the degree of coherence of the coupling is the cooperativity $C = 4g^2/(\kappa\gamma)$, and $C \gg 1$ also represents a criterion for ultrastrong coupling [35,36].

In this paper, we demonstrate that we reach this regime with two types of MMs: Swiss-cross structures representing MMs with a pronounced near-field interaction of unit cells, and split-ring resonators representing MMs with a weak next-neighbor interaction [37]. For the latter, we demonstrate that the measured coupling strength exhibits a square-root dependence on the density of the MM unit cells, as expected from a cavity QED treatment of non-interacting unit cells which are coupled by their collective interaction with the cavity radiation field. We furthermore show that this collective interaction can also occur in a nonlocal way between spatially separated MM layers in the cavity. An analysis of the density dependence of the coupling also allows one to estimate the effective transition dipole moment for single-quantum excitation of the MM plasmonic quasi-particles, which is an intrinsic quantum property which cannot be deduced from a classical electromagnetic field treatment, even though our experiments are conducted with electromagnetic field strengths well into the classical regime at room temperature. This quantity is essential for a description of the collective interaction for future studies employing single photons [31] or entangled photons [32].

2. Results

The inset of Fig. 1(a) illustrates a typical 1D terahertz PC cavity as used in our experiments [13]. It was constructed from five air-gap-separated silicon slabs, a thicker one serving as the central defect layer and two outer pairs with identical thicknesses forming Bragg mirrors on both sides. The first set of measurements were performed with a cavity with a 50-µm-thick defect layer and 23-µm-thick mirror layers with 96-µm air gaps between each Si slab. The transmittance, measured by terahertz time-domain spectroscopy (TDS) with a weakly focused beam, is plotted in Fig. 1(a) (red solid line). One readily discerns a photonic bandgap with a central cavity mode at $\nu_c = \omega_c/2\pi = 0.86$ THz, which is due to the presence of the defect layer. Its full width at half maximum (FWHM) is 10 GHz, corresponding to a Q-factor of 86. Due to high refractive index ratio between Si and air, five Si layers are sufficient to produce a

Optics EXPRESS

high Q-factor cavity mode. The existence of the bandgap and cavity mode are supported by calculations with the transfer matrix method (TMM), see black dashed line in Fig. 1(a) (for a comparison with the measured data over a larger frequency range and a discussion of the differences, see Appendix). In Fig. 1(b), we present the electric field distributions inside the cavity at 0.86 THz, showing the field enhancement. The electric field has two amplitude maxima, resting with opposite polarities on the two surfaces of the defect layer. Hence, qualitatively, one expects a strong electric coupling for any elements placed on a surface of the defect layer.

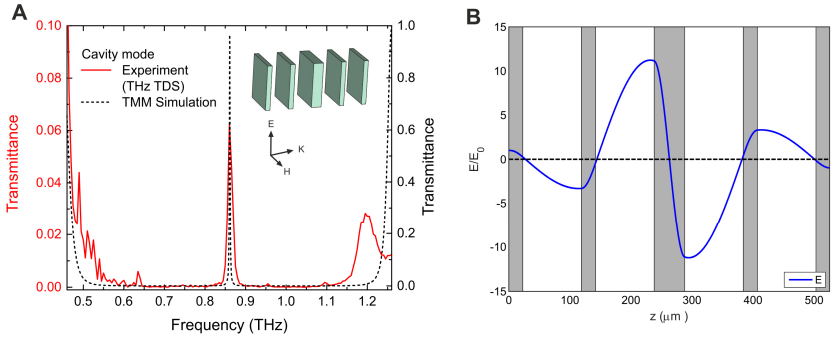

Fig. 1. 1D terahertz PC cavity. (a) Experimental transmittance spectrum of the bare cavity measured by terahertz TDS (solid curve) and corresponding theoretical spectrum calculated with the transfer matrix method (TMM) (dashed curve). The inset shows a typical 1D terahertz PC cavity. (b) Distribution of the electric field within the bare cavity calculated with the TMM. The field strengths are given relative to the field amplitudes E_0 of the incoming radiation. The solid grey rectangles indicate the positions of the Si dielectric layers.

As a first proof-of-principle experiment of cavity-MM coupling via the electric component of the radiation field, we fabricated a regular array of the planar Swiss-cross gold pattern (shown in Fig. 2(a)) directly on one side of the Si defect layer where the electric field enhancement of the standing wave in the cavity is highest. Varying the physical dimensions of the unit cell (x, l, w, as indicated in Fig. 2(a); for values, see Appendix), we prepared six MM specimens with reflection resonance frequencies $\nu_m = \omega_m/2\pi$ ranging from 0.699 to 1.028 THz. The measured transmittance of the free-standing MM (on a Si substrate) with ν_m = 0.895 THz is shown in Fig. 2(b) (black curve), where the reflection resonance manifests as a transmission band-stop filter. The calculated transmittance spectrum of the bare MM is also shown in Fig. 2(b) (red curve; for all MMs, see Fig. 6 in the Appendix). The calculation was performed by employing the commercial Maxwell solver software CST (Dassault Systèmes SE). The FWHM of 244 GHz of the experimental transmittance band is larger than that of the theoretical one, indicating higher conduction losses in Au than assumed in the simulations. The asymmetry of the absorption band is found to be a consequence of the near-field interaction among the unit cells [22]. Also note that the transmission of the symmetric Swiss-cross MM is not sensitive to the polarization of the terahertz radiation.

Figure 2(c) displays measured transmittance spectra of the cavity loaded with each MM (red connected circles). The cavity mode was fixed at 0.86 THz. For all six Swiss-cross specimens, one clearly observes that the cavity mode splits into two hybrid polariton modes. The secondary modes on the high-frequency-side (visible in the lowest three curves in Fig. 2(c)) result from the asymmetry of the MM absorption and are discussed further below.

For the MM with ν_m = 0.841 THz, which is close to the cavity mode resonance at ν_c, the measured polariton mode splitting $2g/2\pi$ amounts to 300 GHz, which yields a normalized coupling strength of $g/\omega_c = 0.17$. With the damping rates for the MM (γ = 244 GHz) and cavity (κ = 10 GHz) derived from the data of Fig. 2(b) (fitted blue dashed curve) and 1b,

Optics EXPRESS

respectively [38,39], one calculates a cooperativity factor $C = 37$. These values demonstrate that our experiment indeed reaches the ultrastrong coupling regime.

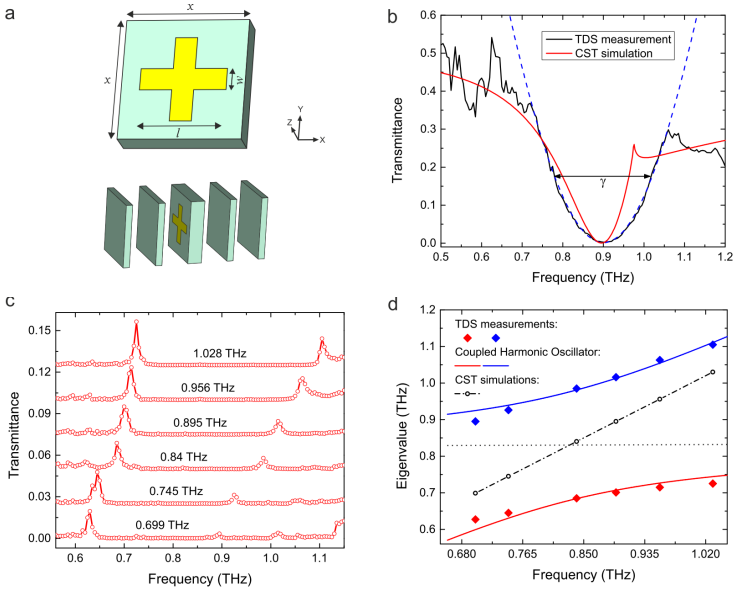

Fig. 2. Strong coupling of Swiss-cross MMs with photons in the cavity. (a) Schematic of the unit cell of the Swiss-cross MM. (b) Transmittance spectrum of the Swiss-cross MM with reflection resonance at $\nu_m = 0.895$ THz (black curve) and theoretical spectrum (red curve). (c) Measured (red connected circles) transmittance spectra of the MM-loaded 1D terahertz cavities for the set of six MMs with varying ν_m. Each spectrum is shifted vertically for visibility. (d) Dispersion of the MM cavity polaritons. Experimental peak frequencies of the upper/lower primary polaritons plotted vs. the theoretical absorption resonance frequency of each bare MM (see (b) and Appendix). Red and blue solid curves: coupled-harmonic-oscillator model.

Figure 2(d) displays the frequencies of the measured primary polariton peaks (the upper branch plotted as blue, the lower one as red diamonds) vs. the frequencies of the absorption resonances of the six MMs. The plot exhibits the typical avoided-crossing behavior of interacting oscillators observed when the resonance frequency of one of them (here the MMs, their frequencies included as open circles connected by the dash-dotted line) is tuned through that of the other one (the cavity, its resonance frequency – assumed here to be 0.83 THz, see Appendix – being plotted as horizontal dotted line).

In analogy to atom-based cavity QED [2], the observed coherent coupling arises from the strong interaction between the cavity photons and the MM plasmons, where the coupling strength is proportional to the vacuum electric field and the square root of the oscillator strength (the latter depending linearly on both the density of the MM unit cells and the square of the effective dipole matrix element). On the other hand, the intuitive classical-physics picture views the interaction as the coherent coupling between two classical harmonic oscillators [40,41]. Employing this latter model (see Appendix), we arrive at the pair of eigenfrequency functions $\omega_\pm$ plotted as red and blue curves in Fig. 2(d), which show good agreement with the experimental data.

In contrast to cavity-QED with a dilute gas of real atoms, where the atoms are essentially isolated from each other and affect each other only weakly (in the absence of cavity feedback), each unit cell of the bare Swiss-cross MM is significantly affected by the adjacent unit-cell structures. This interaction was already found to be responsible for the asymmetry of the absorption band (see Fig. 2(b)). Another consequence of unit-cell interaction is the appearance of secondary polariton resonances in the cavity experiments. In Fig. 2(c), one

Optics EXPRESS

observes them at 1.13, 1.05 and 1.01 THz, for the MMs with ν_m = 0.841, 0.745 and 0.699 THz, respectively. In order to reduce direct interaction between adjacent unit cells and put the focus on the strong coupling of the MMs with cavity photons, we designed MMs based on split-ring resonator (SRR) structures, where inter-cell interactions are known to be much weaker. This is evidenced by the fact that the resonance frequency depends only weakly on the period of the SRR MM [37]. We first present the polariton splitting as a function of the detuning between ν_m and ν_c, by varying the unit cell parameters of the SRR MM (as per the Swiss-cross MM above). A schematic of the unit cell is shown in Fig. 3(a), where the electric component of the cavity field couples to the SRR via the electric dipole across the SRR gap (i.e. polarized along the X-direction). The structural parameters of the fabricated MMs can be found in the Appendix. Figure 3(b) shows the simulated transmittance spectra for each free-standing SRR MM (on Si substrates). The resonance frequency of the SRR changes from 0.64 to 0.99 THz. Figure 3(c) presents the transmittance spectra measured when the SRRs were positioned in the cavity. The spectra again clearly show the splitting of the cavity mode (resonance frequency of bare cavity is 0.86 THz) into two polariton modes. In this case, no secondary polariton modes were observed at other frequencies in the photonic band gap region, due to the much weaker interaction between adjacent unit cells. The extracted peak positions of the two polariton modes are plotted vs. the resonance frequency ν_m of the free-standing SRR MM in Fig. 3(d). The anti-crossing behavior is again reproduced using the coupled-harmonic-oscillator model. The measured mode splitting is 175 GHz, yielding a normalized coupling strength of $g/\omega_c = 0.1$.

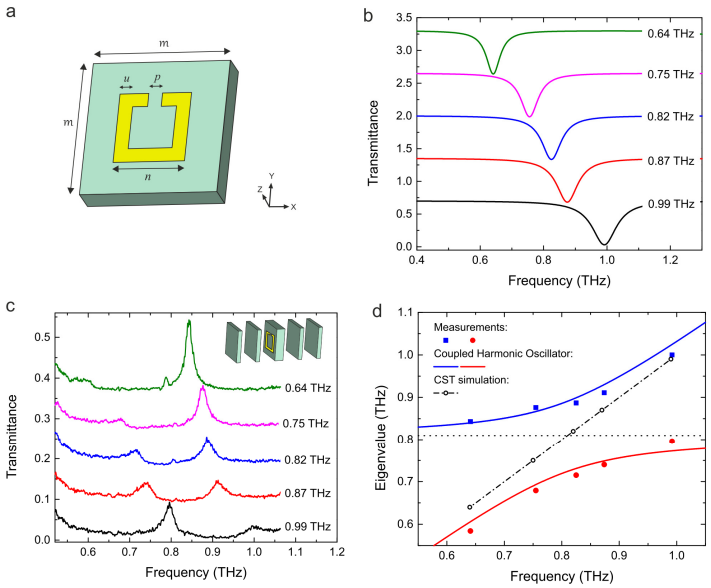

Fig. 3. Strong coupling of SRR MMs with photons in the cavity. (a) Scheme of the SRR unit cell. (b) Calculated transmittance spectra of each SRR MM on Si surface. (c) Measured transmittance spectra with the SRRs positioned in the cavity, with the cavity mode fixed at 0.86 THz. Note that the weak spurious peaks at 0.79-0.8 THz are due to a small polarization leakage along the Y direction. (d) Extracted polariton resonance frequencies (solid circles and squares) from the measured spectra in (c) and fitted curves using the coupled-harmonic-oscillator model (solid red and blue curves).

In order to verify that the strong coupling originates from the enhanced electric field strength on the surface of the defect layer, we carried out a control experiment where the MM was placed in the center of the cavity, where the electric field of the cavity mode is zero (standing-wave node position as seen in Fig. 1(b)). In that case, only the bare cavity mode

Optics EXPRESS

was observed, and no polariton pair was recorded (data shown in the Appendix), confirming that the mode splitting indeed originates from the strong interaction between MM plasmons and the electric field of the photons.

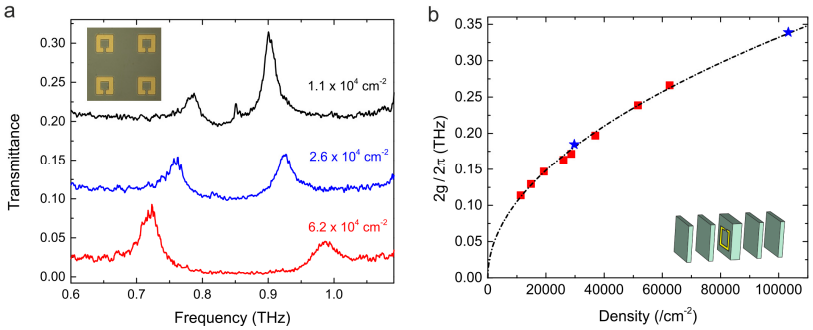

Fig. 4. Nonlocal collective interaction of SRR MMs with cavity photons. (a) Experimental transmittance spectra of coupled plasmon-photon modes for three different unit cell densities. The inset shows an AFM photograph of a part of the processed sample. (b) Dependence of Rabi splitting on SRR unit cell density. The red squares show the Rabi splitting obtained with a single MM layer in the cavity, while the blue stars are for the case of two layers of MMs in the cavity; the dash-dotted line represents a square-root fit.

According to cavity QED with a dilute atomic gas, the coupling strength is proportional to the square root of the number of atoms which participate in the interaction [13]. For the strong coupling with MM, one expects to observe an equivalent dependence. In order to perform such an investigation, we chose SRR MMs because – in contrast to the Swiss Cross MMs – they exhibit weak near-field inter-unit-cell coupling and hence behave more like non-interacting atoms. By keeping the size of the metallic structure of the SRR fixed and only varying the period of the lattice, the effective dipole moment of the SRR unit cell is fixed, but the density of the SRR unit cells varies.

We prepared eight variants of SRR MMs with different unit-cell density on one surface of the defect layer (the structural parameters can be found in the Appendix). The measured transmittance spectra of the MM-loaded cavity are shown in Fig. 4(a) for three unit-cell densities. One clearly notices that the Rabi splitting widens as the density increases. If one plots the measured Rabi splitting as a function of density (shown in Fig. 4(b)), one finds that the data indeed exhibit a square-root dependence, evidencing the collective interaction of a dilute ensemble of dipoles.

The clear square-root dependence is the proof that the effective quantum transition dipole moment μ_{MM} of the SRR quasi-particles remains constant upon variation of the period of the lattice. The Rabi splitting then fulfills $2\hbar g = \sqrt{N}\cdot\mu_{\mathrm{MM}}\cdot E_{\mathrm{vac}}$, where E_{vac} is the vacuum electric field and N is the number of the SRR unit cells in the terahertz beam. Assuming the surface area of the terahertz beam as S_{THz}, and the cavity effect length of the cavity as L_{eff}, one then derives

$$2\hbar g = \sqrt{D_{\mathrm{MM}}S_{\mathrm{THz}}}\cdot\mu_{\mathrm{MM}}\cdot\sqrt{\hbar\omega_0\left(\varepsilon_{\mathrm{r}}L_{\mathrm{eff}}S_{\mathrm{THz}}\right)^{-1}} = \sqrt{D_{\mathrm{MM}}\hbar\omega_0\left(\varepsilon_r L_{\mathrm{eff}}\right)^{-1}}\cdot\mu_{\mathrm{MM}} \qquad (1)$$

where D_{MM} is the 2D SRR unit cell density, and ε_r is the relative permittivity of Si. If one takes the cavity effective length as the inner volume of the cavity (i.e. the thickness of the defect layer and two adjacent air gaps), then the effective transition dipole moment of the SRR quasi-particles can be determined to be $\mu_{\mathrm{MM}} = 1.2\times10^{-23}\,\mathrm{C\cdot m}$, which is several orders of magnitude larger than that of natural atoms (of $6.3\times10^{-30}\,\mathrm{C\cdot m}$ for the 1s-to-2p atomic transition in hydrogen) [42].

Optics EXPRESS

As in natural atoms/molecules, this transition dipole moment is an intrinsic property corresponding to a single quantum of excitation (not to be confused with the classical induced dipole which depends on the field strength), whereby the distance $\delta r = \mu_{\mathrm{MM}}/e$ provides an approximate scale for the displacement of (a unit) charge upon excitation. Here, this results in a value $\delta r = 75\ \mu$m. It is compelling to compare this to the dimensions of the single SRR structure, with an outer ring dimension $n = 24\ \mu$m and stripe width and gap of $u = p = 5\ \mu$m, whereby the length of the SR circuit amounts to $L_{SRR} = 4(n-u) - p = 71\ \mu$m. To our knowledge, this is the first experimental determination of the effective transition dipole moment of a MM unit cell, which is greatly facilitated by the context of cavity coupling and allows this quantity to be calculated from the polariton frequency splitting.

We finally address the nonlocal character of the cavity-MM interaction. For the demonstration of nonlocality, we take advantage of the fact that there are two electric field maxima of the cavity mode, one on each side of the cavity (defect) layer, as shown in Fig. 1(b). We prepared two MM specimens with identical unit-cell density, where a MM layer is located on each side of the defect layer (structural parameters given in the Appendix), and investigated the mode splitting by the coupling with the cavity photons. The measured Rabi splitting is plotted as blue stars in Fig. 4(b). The data points fall nearly perfectly onto the fit curve derived earlier for the single-surface specimens. This experiment clearly demonstrates that the SRR unit cells are still coupled collectively with the photons, even though they originate from spatially separated MM layers (with a separation much larger than the spatial extent of the evanescent fields about each MM layer).

3. Discussion

We have experimentally demonstrated the interaction of photons and plasmonic MMs in a one-dimensional terahertz cavity, and can account for the observed ultrastrong coupling of light-matter interaction using coupled-mode theory. While certain aspects of collective interactions in free-standing MMs have been intensively investigated recently, these rely primarily on a linewidth analysis of the reflection/transmission spectra [43,44]. Here, by exploiting cavity QED, we provide a new experimental approach to study many-body effects in MMs, where the splitting of the cavity-photon-plasmon polaritons provides a robust measure of the collective MM response and quantum properties of each unit cell.

The availability of a broad family of MMs with versatile properties opens the pathway to a range of rich functionalities for the resulting polaritons, such as tunability, polarizability, switchability, and chirality. In addition, the electric field enhancement due to the combined effects of MM and cavity yield a high Q-factor and polariton splitting which can be extremely sensitive to dielectric environmental changes, which can be exploited for applications in chemical and biological sensing [45,46], especially in the terahertz frequency range where many important species have spectroscopic fingerprints. Moreover, one can envisage hybrid cavities, where the plasmon-phonon polaritons additionally couple to fermionic material systems, such as quantum wells or superconductor qubits [47] for quantum information processing.

Appendix

Transmittance of the bare 1D terahertz PC cavity

The cavities were constructed from 10×10-mm^2 pieces of commercially available, highly resistive silicon wafers (purchased with the specified thicknesses and already polished on both sides, specific resistance: $\rho > 5$ kΩ·cm). The four pieces of the mirror slabs were cut from a single wafer to minimize the thickness variation. The wafers were mounted between metallic rings which provide the air spaces. The inner diameter of the metal spacer was 6 mm and the outer diameter 13 mm. The thickness of the metal rings used for all samples varied in

Optics EXPRESS

the range 95-99 μm: the effect of such a variation on the Q-factor of the cavity can be neglected, as confirmed by simulations.

The experimental and simulated transmittance spectra of the 1D terahertz PC cavity in the frequency range about the photonic bandgap region is shown in Fig. 1(b) in the main paper. Here we display these data over a wider spectral range in Fig. 5. The 1D terahertz PC cavity is composed of 23-μm-thick Si outer layers, with 96-μm-thick air spacers and a 50 μm-thick Si defect layer. This design yields the two lowest-order cavity band gaps in the ranges ~0.5-1.25 THz and ~2.25-2.8 THz, respectively, each with a sharp defect pass-band (at ~0.86 and 2.55 THz, respectively). As can be seen, the overall correspondence between theory and experiment is good, although the experimental features are less sharp. For instance, while the calculated Q-factor of the cavity mode at 0.86 THz is 500, in the experimental measurements the Q-factor is only 86. We attribute this effect primarily to the bending of the thin 23-μm Si layers which occurs during construction of the cavity.

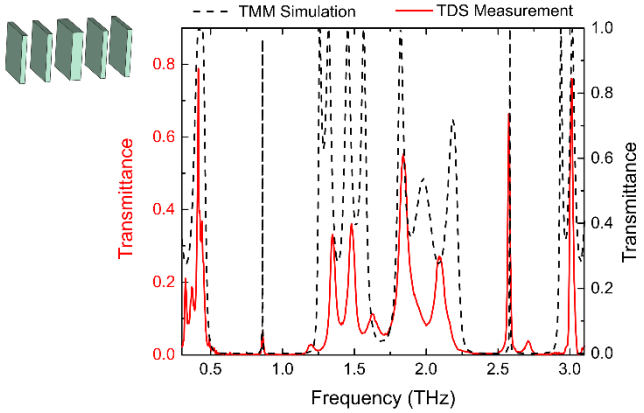

Fig. 5. The simulated (black dashed curve) and measured (red solid curve) transmittance of the 1D terahertz PC cavity (structure as shown).

Experimental setups

We used THz time-domain spectroscopy to characterize the transmittance properties of the bare cavity, the bare MMs and the MM-loaded cavity. In the measurement set-up, terahertz pulses are generated by a two-color air plasma source [48], which is pumped by near-infrared pulses from a Ti:sapphire amplifier laser (Clark-MXR, CPA-2101, 1 kHz, λ_0 = 775 nm, $T_{\mathrm{FWHM}} = 150\,\mathrm{fs}$). The terahertz pulses are detected electro-optically with a 500-μm-thick ZnTe crystal. The optical gating pulse used for electro-optic detection is split from the amplifier laser beam, then spectrally broadened by self-phase-modulation in an argon-filled hollow-core fiber, and temporally compressed down to ~30 fs by a set of negative-dispersion mirrors [49]. The spectral resolution of the measurements is 5 GHz, limited by the time domain scanning range of 200 ps.

For characterizing the transmittance features of SRR MMs, we employed a TOPTICA TeraScan 1550 radiation source. It generates continuous-wave terahertz radiation in an InGaAs photomixer pumped with the beat-note of two telecom lasers (1550 nm) with a tunable difference frequency. The terahertz wave was detected by an InGaAs photoconductive antenna with phase-sensitive photocurrent acquisition.

In both the terahertz spectroscopy setups, the terahertz beam is focused by 100-mm focal length parabolic mirrors, with the focused terahertz beam diameter of ~2 mm. Hence there are ~657 (297) MM unit cells illuminated by the terahertz beam for the smallest (largest) unit cell with the period of 78 μm (116 μm).

Optics EXPRESS

Transmittance of free-standing Swiss-cross metamaterials

Six Swiss-cross MM specimens were fabricated on 50-μm-thick Si substrates which were then inserted into the cavity as MM-loaded defect layers. The metal patterns were defined by optical lithography following the deposition of 5-nm Ti and 200-nm Au by electron-beam evaporation. The pattern transfer was performed by a lift-off process. The frequencies of the absorption resonances of the MMs were selected by the choice of the values of the three parameters x, l, and w of Fig. 2(a). The values are listed in Table 1 (the ratio of the parameters were kept constant).

We present the simulated transmittance spectra of the free-standing MM (on a Si substrate) in Fig. 6 assuming the MM structure to consist of 200-nm-thick Au with a conductivity of 4.56×10^7 S/m (and suppressing multiple reflections in the Si substrate using open boundary conditions). As can be seen, each MM has near-unity transmittance at low frequencies, followed by a resonance-like transmittance minimum with a width ~100 GHz. We classify each MM by their respective resonance frequencies ν_m where the transmission minima occur (i.e. with ν_m ranging from 0.699 to 1.028 THz).

Table 1. Dimensions of the processed Swiss-cross MMs and the calculated resonance frequencies.

Metamaterial type	x	l	w	ν_m
	(μm)	(μm)	(μm)	(THz)
MM	116	81	21	0.699
MM	108	76	19	0.745
MM	96	67	17	0.841
MM	90	63	16	0.899
MM	84	59	15	0.956
MM	78	55	14	1.028

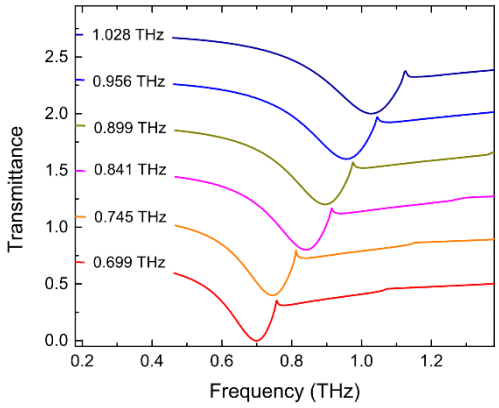

Fig. 6. Simulated transmittance spectra of the free-standing Swiss-cross MM samples used in the experiments, with different MM reflection resonance frequencies ν_m (indicated by the labels for each curve) achieved by varying the MM dimension parameters (see Table 1). The curves are shifted vertically for better visibility.

Strong coupling with Swiss-cross MM positioned in the center of the cavity

We demonstrated the strong coupling of Swiss-cross MM with the electric field of the cavity photon by positioning the Swiss-cross MM on the surface of the defect layer. For comparison, we performed additional control experiments with a MM placed in the center of the defect layer, where the standing-wave electric field is zero.

Optics EXPRESS

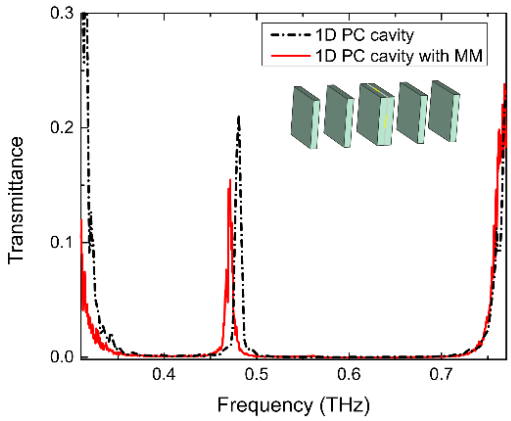

Fig. 7. Experimental transmittance spectra for the bare cavity (black dash-dot line) and MM-loaded cavity (red line).

To realize this geometry, we fabricated a Swiss-cross MM and integrated it into the center of the defect layer by photolithographic preparation of the MM on a Si substrate with half the thickness of the target defect layer, placed in contact with a second substrate to form the sandwiched MM defect layer. Considering the cavity used in the main text, this implied processing a 25-µm-thick Si dielectric substrate. However, performing optical lithography on such a thin Si layer turned out to be extremely challenging, such that we decided to rather work with a sandwich of two 50-µm-thick Si layers. To accommodate the thicker defect layer (i.e. to achieve a defect resonance in the bandgap of the outer Si pairs), we redesigned the cavity using 50-µm-thick Si slabs as dielectric mirror layers separated by air gaps of 96 µm width. Calculations predict the cavity resonance frequency to be at 0.48 THz which was confirmed by transmittance measurement with a tunable continuous-wave THz system, as shown in Fig. 7 (black dash-dot line). The Q-factor of the cavity was found to be 44.

We prepared a Swiss-cross MM in this demonstration, and the size parameters of the MM are $x = 125$ µm, $l = 87$ µm and $w = 22$ µm. The measured transmittance spectrum with the MM loaded in the cavity is shown as the red line in Fig. 7. One clearly notices only one transmission peak in the photonic crystal band gap, and no polariton peak is observed. The slight deviation of the resonance frequency with the MM in the cavity can be attributed to the additional space between two sandwiched Si layers due to the presence of the metallic structure. These experiments indicate that the polariton splitting observed in the main text indeed originates from the strong interaction between the MM and the electric field components of the cavity photons.

Plasmon-photon-polariton with SRR MM

We demonstrate here, that a split-ring-resonator (SRR) MM can also couple strongly with the cavity photons. Employing the same strategy as for the Swiss-cross experiments, we fixed the cavity mode frequency at 0.86 THz, and tuned the resonance frequency ν_m of the SRR MM by varying its structural parameters. A scheme of the SRR MM unit cell is shown in Fig. 3(a) and the respective dimensions are listed in Table 2. The probing electric field was aligned along the X- direction. Figure 3(b) shows the simulated transmittance spectra for each SRR MM on the Si surface. The resonance frequencies of the SRR MMs change from 0.64 to 0.99 THz.

Optics EXPRESS

Table 2. Dimensions of the designed SRR MM (see Fig. 3(a)) and their calculated resonance frequencies ν_m.

Metamaterial type	m	n	u	p	ν_m
	(μm)	(μm)	(μm)	(μm)	(THz)
SRR	75	30	5	5	0.64
SRR	66	26.6	5	5	0.75
SRR	62	25	5	5	0.82
SRR	59	24	5	5	0.87
SRR	55	22	5	5	0.99

For the investigation of the collective interaction of SRR unit cells with cavity photons, the size parameters of the SRR n, u, p were fixed at 24 μm, 5 μm and 5 μm, respectively. We then varied the period m choosing the values 94, 82, 72, 62, 52, 44, and 40 μm. The unit cell density correspondingly varied from $1.1\times10^4\,\mathrm{cm}^{-2}$ to $6.2\times10^4\,\mathrm{cm}^{-2}$.

For the experiments of nonlocal collective interaction, we deposited identical MM layers on each side of the defect layer, which was then placed into the cavity. For the two measurements presented in Fig. 4, we fabricated two different samples, with periods m of 82 and 44 μm, respectively.

Rabi splitting versus absolute terahertz pulse intensity

Note that because MM plasmons represent a bosonic system, the Rabi splitting does not depend on the number of photons coupled externally into the cavity [50]. We tested this assertion by experimental variation of the incident terahertz pulse intensity, which left the Rabi splitting unchanged as expected. While this feature justifies the description of the system by coupled harmonic oscillators, this harmonic character must be broken to make applications in quantum information processing possible. Several pathways to achieve this have been suggested in the literature such as active feedback in the cavity [51] which poses a promising avenue for future investigations.

Classical theory of coupled harmonic oscillators

We simulated the dependence of the polariton splitting (and avoid-crossing behavior) on the Swiss-cross MM resonance frequency (Fig. 2(d)) within the coupled harmonic oscillator formalism [41], which is based on differential equations for the two generalized coordinates $x_1(t)$ and $x_2(t)$:

$$\begin{aligned} \ddot{x}_1 + \kappa\dot{x}_1 + \omega_c^2 x_1 + V\dot{x}_2 &= 0 \\ \ddot{x}_2 + \gamma\dot{x}_2 + \omega_m^2 x_2 - V\dot{x}_1 &= 0, \end{aligned} \tag{2}$$

where ω_c is the cavity mode frequency, ω_m the MM resonance frequency, κ the photon number decay rate of the cavity, γ the damping rate of the MM plasmons, and, V the coupling parameter. Under the conditions $\omega^2-\omega_c^2 \approx -2\omega(\omega_c-\omega)$ and $\omega^2-\omega_m^2 \approx -2\omega(\omega_m-\omega)$, one obtains solutions with the following frequency eigenvalues:

$$\begin{aligned} \omega_\pm = &(\frac{\omega_c+\omega_m}{2}) - i(\frac{\kappa+\gamma}{4}). \\ &\pm\frac{1}{2}\sqrt{(\omega_m-\omega_c)^2 - (\frac{\kappa-\gamma}{2})^2 + i(\frac{\kappa-\gamma}{2})(\omega_m-\omega_c) + V^2} \end{aligned} \tag{3}$$

Optics EXPRESS

By employing the experimental damping rates (κ and γ , given in the main text), we obtained the fit shown in Fig. 2(d), which yielded an estimate for the coupling parameter $V = 300$ GHz. Note that the cavity mode frequency had to be taken as 0.83 THz (instead of 0.86 THz) in order to restore the experimental inversion symmetry of the two polariton branches with respect to the $\omega_c = \omega_m$-point (crossing point of the two lines in Fig. 2(d)). The effective resonance shift is attributed to a slight change of the cavity parameters either induced by the finite thickness of the MM's metallization or occurring during cavity alignment. For the simulation of SRR MM as shown in Fig. 3(d), we employed a similar method.

Funding

The HessenFonds of the Hessian Ministry for Science and the Arts; the European Union via project CELTA (a project of the Training Networks program).

Acknowledgments

The authors thank Alvydas Lisauskas, Bernd Hils, and Amin Soltani for their help with the experiments.

Disclosures

The authors declare that there are no conflicts of interest related to this article.

References

1. C. Gerry and P. Knight, Introductory Quantum Optics (Cambridge University Press, 2004).
2. H. Walther, B. T. H. Varcoe, B.-G. Englert, and T. Becker, "Cavity quantum electrodynamics," Rep. Prog. Phys. **69**(5), 1325–1382 (2006).
3. S. J. van Enk, H. J. Kimble, and H. Mabuchi, "Quantum information processing in cavity-QED," Quantum Inform. Process. **3**(1-5), 75–90 (2004).
4. S. Haroche, "Nobel lecture: controlling photons in a box and exploring the quantum to classical boundary," Rev. Mod. Phys. **85**(3), 1083–1102 (2013).
5. J. M. Raimond, M. Brune, and S. Haroche, "Manipulating quantum entanglement with atoms and photons in a cavity," Rev. Mod. Phys. **73**(3), 565–582 (2001).
6. D. Dini, R. Köhler, A. Tredicucci, G. Biasiol, and L. Sorba, "Microcavity polariton splitting of intersubband transitions," Phys. Rev. Lett. **90**(11), 116401 (2003).
7. C. Weisbuch, M. Nishioka, A. Ishikawa, and Y. Arakawa, "Observation of the coupled exciton-photon mode splitting in a semiconductor quantum microcavity," Phys. Rev. Lett. **69**(23), 3314–3317 (1992).
8. S. Brodbeck, S. De Liberato, M. Amthor, M. Klaas, M. Kamp, L. Worschech, C. Schneider, and S. Höfling, "Experimental verification of the very strong coupling regime in a GaAs quantum well microcavity," Phys. Rev. Lett. **119**(2), 027401 (2017).
9. J. P. Reithmaier, G. Sek, A. Löffler, C. Hofmann, S. Kuhn, S. Reitzenstein, L. V. Keldysh, V. D. Kulakovskii, T. L. Reinecke, and A. Forchel, "Strong coupling in a single quantum dot-semiconductor microcavity system," Nature **432**(7014), 197–200 (2004).
10. H. Groß, J. M. Hamm, T. Tufarelli, O. Hess, and B. Hecht, "Near-field strong coupling of single quantum dots," Sci. Adv. **4**(3), r4906 (2018).
11. A. Wallraff, D. I. Schuster, A. Blais, L. Frunzio, R. Huang, J. Majer, S. Kumar, S. M. Girvin, and R. J. Schoelkopf, "Strong coupling of a single photon to a superconducting qubit using circuit quantum electrodynamics," Nature **431**(7005), 162–167 (2004).
12. G. Scalari, C. Maissen, D. Turcinková, D. Hagenmüller, S. De Liberato, C. Ciuti, C. Reichl, D. Schuh, W. Wegscheider, M. Beck, and J. Faist, "Ultrastrong coupling of the cyclotron transition of a 2D electron gas to a THz metamaterial," Science **335**(6074), 1323–1326 (2012).
13. Q. Zhang, M. Lou, X. Li, J. L. Reno, W. Pan, J. D. Watson, M. J. Manfra, and J. Kono, "Collective non-perturbative coupling of 2D electrons with high-quality-factor terahertz cavity photons," Nat. Phys. **12**(11), 1005–1011 (2016).
14. H. Huebl, C. W. Zollitsch, J. Lotze, F. Hocke, M. Greifenstein, A. Marx, R. Gross, and S. T. B. Goennenwein, "High cooperativity in coupled microwave resonator ferrimagnetic insulator hybrids," Phys. Rev. Lett. **111**(12), 127003 (2013).
15. X. Zhang, C. L. Zou, L. Jiang, and H. X. Tang, "Cavity magnomechanics," Sci. Adv. **2**(3), e1501286 (2016).
16. X. Zhang, C. L. Zou, L. Jiang, and H. X. Tang, "Strongly coupled magnons and cavity microwave photons," Phys. Rev. Lett. **113**(15), 156401 (2014).
17. A. Shalabney, J. George, J. Hutchison, G. Pupillo, C. Genet, and T. W. Ebbesen, "Coherent coupling of molecular resonators with a microcavity mode," Nat. Commun. **6**(1), 5981 (2015).

Optics EXPRESS

18. R. Chikkaraddy, B. de Nijs, F. Benz, S. J. Barrow, O. A. Scherman, E. Rosta, A. Demetriadou, P. Fox, O. Hess, and J. J. Baumberg, "Single-molecule strong coupling at room temperature in plasmonic nanocavities," Nature **535**(7610), 127–130 (2016).
19. A. Christ, S. G. Tikhodeev, N. A. Gippius, J. Kuhl, and H. Giessen, "Waveguide-plasmon polaritons: strong coupling of photonic and electronic resonances in a metallic photonic crystal slab," Phys. Rev. Lett. **91**(18), 183901 (2003).
20. V. G. Kravets, F. Schedin, and A. N. Grigorenko, "Extremely narrow plasmon resonances based on diffraction coupling of localized plasmons in arrays of metallic nanoparticles," Phys. Rev. Lett. **101**(8), 087403 (2008).
21. R. Ameling and H. Giessen, "Microcavity plasmonics: strong coupling of photonic cavities and plasmons," Laser Photonics Rev. **7**(2), 141–169 (2013).
22. W. Cai and V. Shalav, Optical Metamaterials: Fundamentals and Applications (Springer-Verlag, 2010).
23. Z. Wang, F. Cheng, T. Winsor, and Y. Liu, "Optical chiral metamaterials: a review of the fundamentals, fabrication methods and applications," Nanotechnology **27**(41), 412001 (2016).
24. R. A. Shelby, D. R. Smith, and S. Schultz, "Experimental verification of a negative index of refraction," Science **292**(5514), 77–79 (2001).
25. N. I. Landy, S. Sajuyigbe, J. J. Mock, D. R. Smith, and W. J. Padilla, "Perfect metamaterial absorber," Phys. Rev. Lett. **100**(20), 207402 (2008).
26. G. Duan, J. Schalch, X. Zhao, J. Zhang, R. D. Averitt, and X. Zhang, "Identifying the perfect absorption of metamaterial absorbers," Phys. Rev. B **97**(3), 035128 (2018).
27. D. Schurig, J. J. Mock, B. J. Justice, S. A. Cummer, J. B. Pendry, A. F. Starr, and D. R. Smith, "Metamaterial electromagnetic cloak at microwave frequencies," Science **314**(5801), 977–980 (2006).
28. M. Wei, Q. Yang, X. Zhang, Y. Li, J. Gu, J. Han, and W. Zhang, "Ultrathin metasurface-based carpet cloak for terahertz wave," Opt. Express **25**(14), 15635–15642 (2017).
29. E. Altewischer, M. P. van Exter, and J. P. Woerdman, "Plasmon-assisted transmission of entangled photons," Nature **418**(6895), 304–306 (2002).
30. M. S. Tame, K. R. McEnery, S. K. Özdemir, J. Lee, S. A. Maier, and M. S. Kim, "Quantum plasmonics," Nat. Phys. **9**(6), 329–340 (2013).
31. T. Roger, S. Vezzoli, E. Bolduc, J. Valente, J. J. F. Heitz, J. Jeffers, C. Soci, J. Leach, C. Couteau, N. I. Zheludev, and D. Faccio, "Coherent perfect absorption in deeply subwavelength films in the single-photon regime," Nat. Commun. **6**(1), 7031 (2015).
32. T. Stav, A. Faerman, E. Maguid, D. Oren, V. Kleiner, E. Hasman, and M. Segev, "Quantum entanglement of the spin and orbital angular momentum of photons using metamaterials," Science **361**(6407), 1101–1104 (2018).
33. J. Casanova, G. Romero, I. Lizuain, J. J. García-Ripoll, and E. Solano, "Deep strong coupling regime of the Jaynes-Cummings model," Phys. Rev. Lett. **105**(26), 263603 (2010).
34. A. Bayer, M. Pozimski, S. Schambeck, D. Schuh, R. Huber, D. Bougeard, and C. Lange, "Terahertz light–matter interaction beyond unity coupling strength," Nano Lett. **17**(10), 6340–6344 (2017).
35. J. J. Viennot, M. C. Dartiailh, A. Cottet, and T. Kontos, "QUANTUM INFORMATION. Coherent coupling of a single spin to microwave cavity photons," Science **349**(6246), 408–411 (2015).
36. Y. Tabuchi, S. Ishino, T. Ishikawa, R. Yamazaki, K. Usami, and Y. Nakamura, "Hybridizing ferromagnetic magnons and microwave photons in the quantum limit," Phys. Rev. Lett. **113**(8), 083603 (2014).
37. R. Singh, C. Rockstuhl, and W. Zhang, "Strong influence of packing density in terahertz metamaterials," Appl. Phys. Lett. **97**(24), 241108 (2010).
38. D. J. Shelton, I. Brener, J. C. Ginn, M. B. Sinclair, D. W. Peters, K. R. Coffey, and G. D. Boreman, "Strong coupling between nanoscale metamaterials and phonons," Nano Lett. **11**(5), 2104–2108 (2011).
39. G. R. Keiser, H. R. Seren, A. C. Strikwerda, X. Zhang, and R. D. Averitt, "Structural control of metamaterial oscillator strength and electric field enhancement at terahertz frequencies," Appl. Phys. Lett. **105**(8), 081112 (2014).
40. B. M. Yao, Y. S. Gui, Y. Xiao, H. Guo, X. S. Chen, W. Lu, C. L. Chien, and C.-M. Hu, "Theory and experiment on cavity magnon-polariton in the one-dimensional configuration," Phys. Rev. B Condens. Matter Mater. Phys. **92**(18), 184407 (2015).
41. L. Novotny, "Strong coupling, energy splitting, and level crossings: A classical perspective," Am. J. Phys. **78**(11), 1199–1202 (2010).
42. M. Fox, Quantum optics: an introduction (Oxford University Press, 2006).
43. V. A. Fedotov, N. Papasimakis, E. Plum, A. Bitzer, M. Walther, P. Kuo, D. P. Tsai, and N. I. Zheludev, "Spectral collapse in ensembles of metamolecules," Phys. Rev. Lett. **104**(22), 223901 (2010).
44. S. D. Jenkins, J. Ruostekoski, N. Papasimakis, S. Savo, and N. I. Zheludev, "Many-body subradiant excitations in metamaterial arrays: experiment and theory," Phys. Rev. Lett. **119**(5), 053901 (2017).
45. H. Tao, L. R. Chieffo, M. A. Brenckle, S. M. Siebert, M. Liu, A. C. Strikwerda, K. Fan, D. L. Kaplan, X. Zhang, R. D. Averitt, and F. G. Omenetto, "Metamaterials on paper as a sensing platform," Adv. Mater. **23**(28), 3197–3201 (2011).
46. C. Wu, A. B. Khanikaev, R. Adato, N. Arju, A. A. Yanik, H. Altug, and G. Shvets, "Fano-resonant asymmetric metamaterials for ultrasensitive spectroscopy and identification of molecular monolayers," Nat. Mater. **11**(1), 69–75 (2011).

Optics EXPRESS

47. Y. Tabuchi, S. Ishino, A. Noguchi, T. Ishikawa, R. Yamazaki, K. Usami, and Y. Nakamura, "QUANTUM INFORMATION. Coherent coupling between a ferromagnetic magnon and a superconducting qubit," Science **349**(6246), 405–408 (2015).
48. M. D. Thomson, V. Blank, and H. G. Roskos, "Terahertz white-light pulses from an air plasma photo-induced by incommensurate two-color optical fields," Opt. Express **18**(22), 23173–23182 (2010).
49. V. Blank, M. D. Thomson, and H. G. Roskos, "Spatio-spectral characteristics of ultra-broadband THz emission from two-colour photoexcited gas plasmas and their impact for nonlinear spectroscopy," New J. Phys. **15**(7), 075023 (2013).
50. I. Chiorescu, N. Groll, S. Bertaina, T. Mori, and S. Miyashita, "Magnetic strong coupling in a spin-photon system and transition to classical regime," Phys. Rev. B Condens. Matter Mater. Phys. **82**(2), 024413 (2010).
51. B. Yao, Y. S. Gui, J. W. Rao, S. Kaur, X. S. Chen, W. Lu, Y. Xiao, H. Guo, K.-P. Marzlin, and C.-M. Hu, "Cooperative polariton dynamics in feedback-coupled cavities," Nat. Commun. **8**(1), 1437 (2017).